

# Radiatively inefficient accretion flows induced by gravitational-wave emission before massive black hole coalescence

Kimitake Hayasaki

*Department of Astronomy, Kyoto University Oiwake-cho, Kitashirakawa, Sakyo-ku, Kyoto 606-8502, Japan*

kimi@kustastro.kyoto-u.ac.jp

## ABSTRACT

We study an accretion flow during the gravitational-wave driven evolution of binary massive black holes. After the binary orbit decays due to an interaction with a massive circumbinary disk, the binary is decoupled from the circumbinary disk because the orbital-decay timescale due to emission of gravitational wave becomes shorter than the viscous timescale evaluated at the inner edge of circumbinary disk. During the subsequent evolution, the accretion disk, which is truncated at the tidal radius because of the tidal torque, also shrinks as the orbital decay. Assuming that the disk mass changed by this process is all accreted, the disk becomes radiatively inefficient when the semi-major axis is several hundred Schwarzschild radii. The high-energy radiations, in spite of a low bolometric luminosity, are emitted from an accretion disk around each black hole long before the black hole coalescence as well as the gravitational wave signals. The synchrotron process can notably produce potentially observable radio emissions at large distances if there is a strong, dipole magnetic field around each black hole. In unequal mass-ratio binaries, step-like light variations are seen in the observed light curve because the luminosity is higher and its duration time are shorter in the radio emission by the disk around the secondary black hole than those of the primary black hole. Such a precursor would be unique to not a single black hole system but a binary black hole system, and implies that binary black holes finally merge without accretion disks.

*Subject headings:* black hole physics - accretion, accretion disks - gravitational waves - galaxies: evolution - galaxies: active - galaxies: nuclei - quasars: general - binaries: general

## 1. Introduction

Astrophysical disks are ubiquitous and sources of active phenomena in the various system of the Universe; the star-compact object systems, star-planet systems, active galactic nuclei (AGNs), and so forth. Although the standard theory of accretion disks (Shakura & Sunyaev 1973) has succeeded in explaining them, there are still many unsolved problems.

High-energy emission from galactic black hole binaries and AGNs cannot be produced by the accretion flow, except for the accretion flow accompanied by a corona, derived from the standard disk theory, where radiative cooling is so efficient that the thermal energy heated up by the viscosity is locally radiated away. If the radiative cooling becomes inefficient, the thermal energy is transported inward with accretion, and then the flow becomes hot. Such a flow can produce high-energy emission and is generally called as radiatively inefficient accretion flow (RIAF) (Chap. 9 of Kato et al. 2008).

The proto-type model of the RIAF is an optically thin advection-dominated accretion flow (ADAF) (Ichimaru 1977; Narayan & Yi 1994, 1995; Abramowicz et al. 1995; see also Chap. 9 of Kato et al. 2008 for a review). A low luminosity with high-energy emission can be explained by the ADAF with a significantly lower accretion rate than  $\dot{M}_E = L_E/c^2 \sim 2 \times 10^{-2} M_7 [M_\odot \text{yr}^{-1}]$ , where  $L_E = 4\pi c G M_{\text{bh}}/\kappa_{\text{es}} \sim 1.3 \times 10^{45} M_7 [\text{ergs}^{-1}]$ ,  $c$ ,  $G$ ,  $M_7$ , and  $\kappa_{\text{es}}$  are the Eddington luminosity, light speed, gravitational constant, black hole mass normalized by  $10^7 M_\odot$ , and electron scattering opacity, respectively. Observed power-law spectra of X-rays from Sgr A\* was well reproduced by ADAFs (Manmoto et al. 1997).

Most galaxies are thought to have massive black holes at their centers (Kormendy & Richstone 1995) and to coevolve with them (Magorrian et al. 1998; Ferrarese & Merritt 2000; Gebhardt et al. 2000). Galaxy merger leads to the mass inflow to the central region and then a nucleus of the merged galaxy is activated and black hole grows by gas accretion. During a sequence of processes, binary massive black holes with a sub-parsec scale separation are inevitably formed before two black holes merge by emitting gravitational radiation (Begelman et al. 1980; Escala et al. 2005; Dotti et al. 2007; Mayer et al. 2007). By interaction with surrounding stars (Merritt & Milosavljević 2005 and references therein; Berentzen et al. 2009), gaseous disks (Ivanov et al. 1999; Gould & Rix 2000; Armitage & Natarajan 2002; Hayasaki 2009; Cuadra et al. 2009; Haiman et al. 2009), other massive black holes (Iwasawa et al. 2006), and infalling dwarf galaxies (Matsui & Habe 2009), the binary evolves towards coalescence within Hubble time, although whether the binary finally coalesces still remains uncertainty theoretically (e.g., Lodato et al. 2009) and observationally. Then, gravitational radiation emitted prior to coalescence is detectable with the *Laser Interferometer Space Antenna* (LISA) and Pulsar Timing Arrays (PTAs).

An electromagnetic counterpart of gravitational wave signal plays a key role in determining the redshift of the source. By combining the redshift with its luminosity distance the gravitational wave determines, one can obtain the distance-redshift relation, which is one of best observational probes of the dark energy (Schutz 1986; Holz&Hughes 2005). Some types of the electromagnetic counterparts have been studied such as afterglows (Milosavljević&Phinney 2005; Rossi et al. 2010; Corrales et al. 2010; Tanaka&Menou 2010) and precursors as the prompt emissions (Chang et al. 2009; Bode et al. 2010; Stone & Loeb 2010) and periodic emissions (Hayasaki et al. 2007, 2008; Bogdanović et al. 2008; MacFadyen & Milosavljević 2008; Hayasaki & Okazaki 2009).

In this Letter, we investigate RIAFs triggered by the rapid orbital decay due to emission of gravitational wave. The letter is organized as follows. The evolution of binary massive black holes interacting with a massive circumbinary disk are briefly described in Section 2. In Section 3, we derive the possible accretion flows and their luminosities during the gravitational-wave driven evolution. Section 4 is devoted to summary and discussion.

## 2. Final Parsec Evolution of Binary Massive Black Holes

We first briefly describe the evolution of binary massive black holes interacting with a massive circumbinary disk in the framework of coevolution of massive black holes and their host galaxies. The detailed description can be seen in Hayasaki et al. (2010).

Binary black holes are considered mainly to evolve via three stages (Begelman et al. 1980). Firstly, each of black holes sinks independently towards the center of the common gravitational potential due to the dynamical friction with neighboring stars. When the separation between two black holes becomes less than 1 pc or so, angular momentum loss by the dynamical friction slows down due to the loss-cone effect and a massive hard binary is formed. This is the second stage. The binary hardens at the radius where the kinetic energy per unit mass of the star with the velocity dispersion equals to the binding energy per unit mass of binary black holes (Quinlan 1996). Its hardening radius is defined as  $a_h \sim 8.5 \times 10^{-1} [\text{pc}] (q/(1+q)^2) M_7^{1-2/\beta_2}$ , where  $q = M_s/M_p$  is the ratio of primary black-hole mass,  $M_p$ , to secondary black-hole mass,  $M_s$ . Here, it is assumed that the total black-hole mass is tightly correlated with the velocity dispersion:  $M_7 = \beta_1 (\sigma_*/200 \text{ km s}^{-1})^{\beta_2}$  with  $\beta_1 = 16.6$  and  $\beta_2 = 4.86$ , where  $\sigma_*$  shows the one-dimensional velocity dispersion of stars (Merritt & Milosavljević 2005). Finally, the semi-major axis of the binary decreases to the radius at which the gravitational radiation dominates, and then a pair of black holes merge into a single, more massive one.

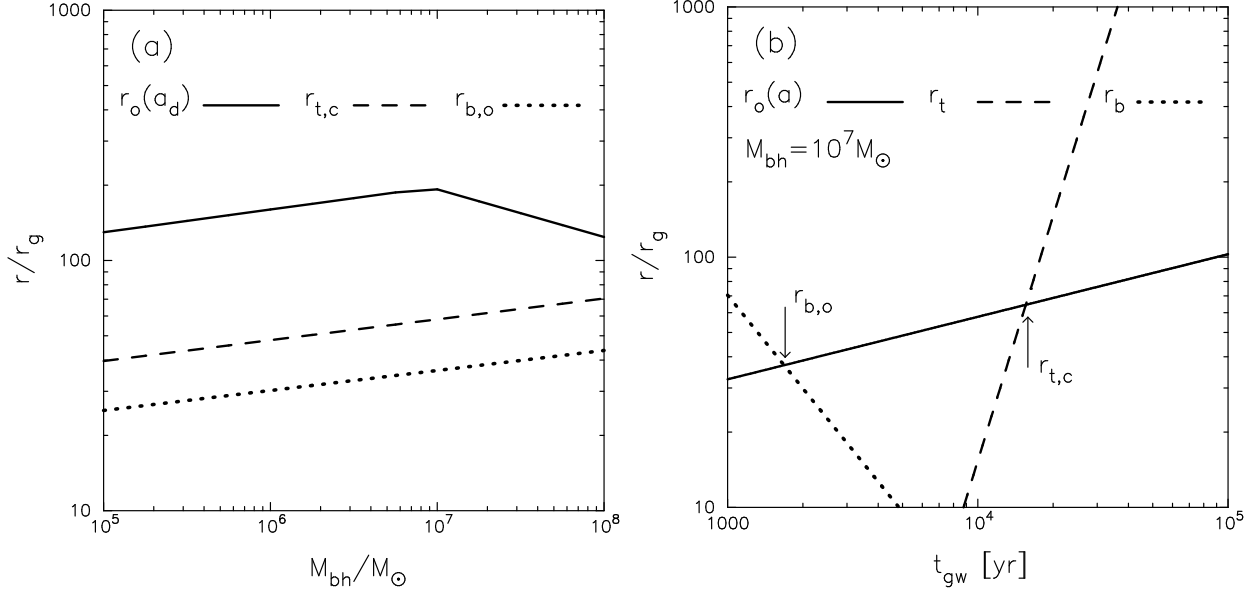


Fig. 1.— (a) Black-hole mass dependence of characteristic radii of the accretion disk around the primary black hole in the binary with  $q = 0.1$ . The solid line represents the tidal radius when the binary is decoupled from the circumbinary disk. The dashed line shows the critical transition radius,  $r_{t,c}$ , where the disk-outer edge corresponds to the transition radius,  $r_t$ , from the standard disk to the RIAF. The dotted line shows the radius,  $r_{b,o}$ , where the disk-outer edge corresponds to the boundary,  $r_b$ , between the inner, radiation-pressure dominated region and the middle, gas-pressure dominated region. (b) Evolution of characteristic radii for  $M_{bh} = 10^7 M_\odot$ . The solid line, dashed line, and dotted line represent the disk-outer edge,  $r_o(a)$ ,  $r_t$ , and  $r_b$ , respectively. The intersection between the solid line and the dashed line shows  $r_{t,c}$ , whereas the one between the solid line and the dotted line shows  $r_{b,o}$ .

## 2.1. Triple-Disk Evolution

The circumbinary disk would be formed around hardening of the binary. The inner edge of circumbinary disk,  $r_{in}$ , is then defined as  $r_{in} \approx 2a \sim 1.8[\text{pc}](q/(1+q)^2)M_7^{1-2/\beta_2}(a/a_h)$ , where  $a$  is the semi-major axis of binary. For simplicity, the circumbinary disk is assumed to be a steady, axisymmetric, geometrically thin, self-regulated, self-gravitating but non-fragmenting with a Keplerian rotation and accretion rate,  $\dot{M}_{acc} = (\eta/\epsilon)\dot{M}_{Edd}$ , with the Eddington ratio,  $\eta$ , mass-to-energy conversion efficiency,  $\epsilon$ , and Shakura-Sunyaev type viscosity parameter,  $\alpha_{sg}$ .

The circumbinary disk and binary exchanges the energy and angular momentum through

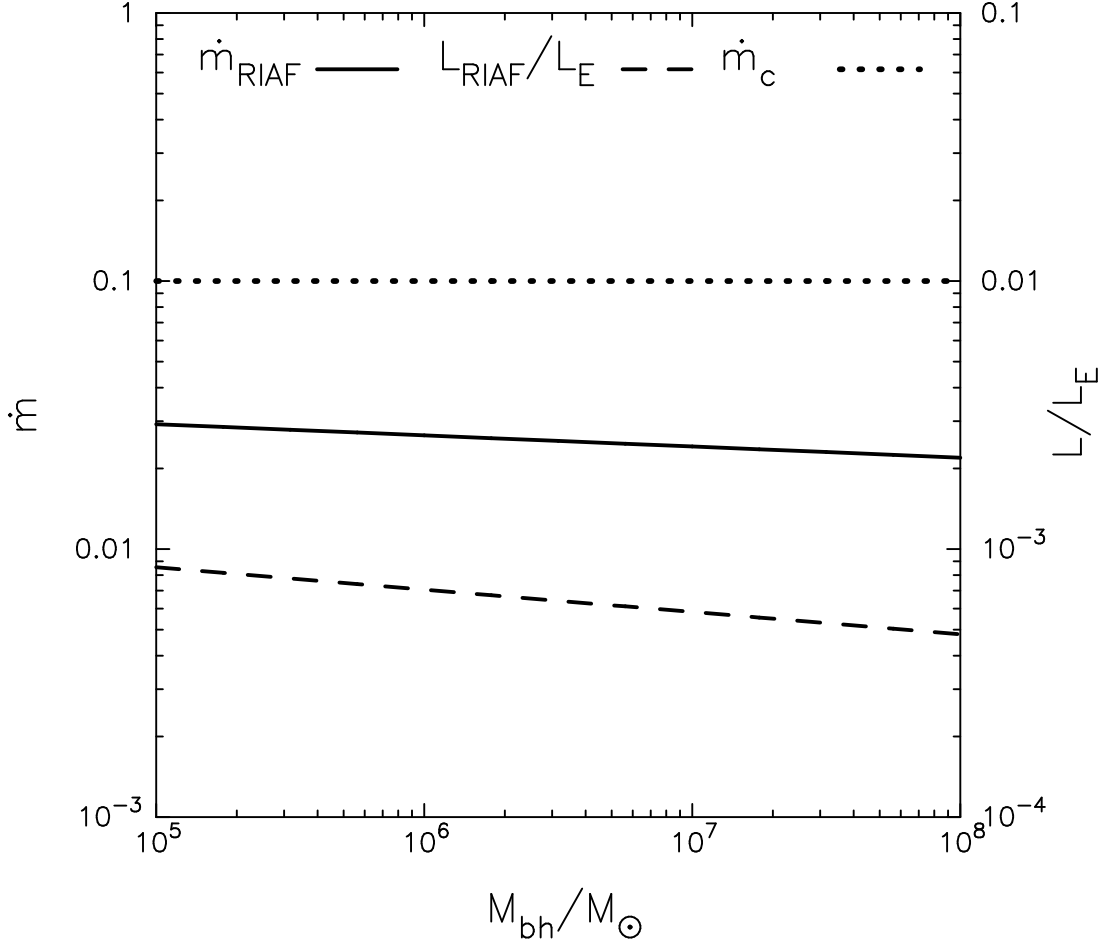


Fig. 2.— Black-hole mass dependence of the normalized accretion rate and corresponding normalized luminosity in the binary with  $q = 0.1$ . The normalized accretion rate,  $\dot{m}_{\text{RIAF}}$ , is evaluated at the critical transition radius,  $r_{\text{t,c}}$ . The solid line and dashed line show  $\dot{m}_{\text{RIAF}}$  and corresponding normalized luminosity,  $L_{\text{RIAF}}/L_{\text{E}}$ , respectively. The dotted line shows the normalized critical accretion rate,  $\dot{m}_{\text{c}}$ .

the tidal/resonant interaction, which leads to the orbital decay of the binary. On the other hand, the gas at the inner edge of circumbinary disk overflows onto the central binary (Hayasaki et al. 2007). Then, an accretion disk is formed around each black hole (Hayasaki et al. 2008). The mass transfer therefore adds its angular momentum to the binary via accretion disks (Hayasaki 2009). In a steady state, the mass transfer rate equals to  $\dot{M}_{\text{acc}}$ . Since it is much smaller than the critical transfer rate defined by equation (41) of Hayasaki (2009), the additional torque to the binary by the mass transfer can be neglected. The orbital-decay timescale is then given as  $t_{\text{gas}} \sim 3.1 \times 10^8 [\text{yr}] (q/(1+q)^2) \eta_{0.1}^{-1} \epsilon_{0.1}$ , where  $\eta_{0.1} = \eta/0.1$  and  $\epsilon_{0.1} = \epsilon/0.1$ . The total mass supplied to the central binary during the orbital decay is

obtained as

$$M_{\text{sup}} = \dot{M}_{\text{acc}} t_{\text{gas}} \sim 6.2 \times 10^6 [M_{\odot}] M_7 \frac{q}{(1+q)^2}. \quad (1)$$

$M_{\text{sup}}$  thus gives an upper limit of mass of two accretion disks.

### 2.1.1. Decoupling of Circumbinary Disk

The orbital-decay timescale of the binary by gravitational-wave emission can be written by Peters (1964) as

$$t_{\text{gw}} = \left| \frac{a}{\dot{a}} \right|_{\text{gw}} = \frac{5}{8} \left( \frac{a}{r_g} \right)^4 \frac{r_g}{c} \frac{(1+q)^2}{q} \frac{(1-e^2)^{7/2}}{f(e)}, \quad (2)$$

where  $e$  is the orbital eccentricity,  $f(e) = (1 + 73e^2/24 + 37e^4/96)$  is a function of the orbital eccentricity, and  $r_g = 2GM_{\text{bh}}/c^2$  is the Schwarzschild radius of total black hole mass. For simplicity, the orbital eccentricity set to be zero, unless otherwise noted, in what follows.

As the binary evolves, the circumbinary disk behaves as the standard disk in the inner region for  $M_{\text{bh}} \lesssim 10^7 M_{\odot}$ , whereas the disk still remains to be self-gravitating for  $M_{\text{bh}} \gtrsim 10^7 M_{\odot}$ . When the orbital-decay timescale is shorter than the viscous timescale measured at the inner edge of the circumbinary disk, the binary is decoupled from the circumbinary disk. For the self-gravitating disk, the decoupling radius can be defined as  $a_d/r_g = [(8/5)(ct_{\text{vis,g}}/r_g)(q/(1+q)^2)]^{2/7}$ , where  $t_{\text{vis,g}} \sim 5.6 \times 10^4 [\text{yr}] (\alpha_{\text{sg}}/0.06)^{-1/3} \eta_{0.1}^{2/3} \epsilon_{0.1}^{2/3} M_7^{1/3}$  is the viscous timescale measured at  $a = r_g$  (Hayasaki et al. 2010). For the standard disk,  $a_d/r_g = [(8/5)(ct_{\text{vis,g}}/r_g)(q/(1+q)^2)]^{4/11}$ , where  $t_{\text{vis,g}} \sim 5.9 \times 10^2 [\text{yr}] (\alpha_{\text{ss}}/0.1)^{-1} \eta_{0.1}^{-1/4} \epsilon_{0.1}^{1/4} M_7^{5/4}$ . After the binary is decoupled from the circumbinary disk, the system consists of only an accretion disk around each black hole.

## 3. Subsequent Double-Disk Evolution

For simplicity, we focus on the accretion disk around the primary black hole in what follows. Assuming that the binary has a circular orbit, the disk outer edge can be defined by the tidal radius as  $r_o(a) \simeq 0.9R_1 \sim 4.2 \times 10^{-1} (M_p/M_{\text{bh}})^{1/3} a$ , where  $M_{\text{bh}} = M_p + M_s$  and  $R_1$  shows the inner Roche radius of the primary black hole for  $q \gtrsim 0.1$  (e.g., Frank et al. 2002). The logarithmic differentiation of the tidal radius is given by

$$\frac{\dot{r}_o(a)}{r_o(a)} = \frac{\dot{a}}{a} + \frac{1}{3} \frac{q}{1+q} \left[ \frac{\dot{M}_p}{M_p} - \frac{\dot{M}_s}{M_s} \right] \approx \frac{\dot{a}}{a}, \quad (3)$$

where  $\dot{M}_p$  and  $\dot{M}_s$  are the growth rate of primary black hole and that of secondary black hole, respectively.  $\dot{M}_p/M_p \ll 1$  and  $\dot{M}_s/M_s \ll 1$  are held during the evolution.

The accretion disk, which is truncated at the tidal radius because of its tidal torque, shrinks with the orbital decay due to gravitational-wave emission. The disk mass lying between  $r + \Delta r$  and  $\Delta r$  can be then estimated as

$$\Delta M = 2\pi \int_r^{r+\Delta r} \Sigma(r) r dr \approx 2\pi r \Sigma(r) \Delta r. \quad (4)$$

We assume that the disk mass changed by shrinking of the tidal radius steadily accretes onto the black hole without being emitted as jet or wind. Combining equation (4) with equations (2) and (3), we obtain the accretion rate normalized by  $\dot{M}_E$ :

$$\dot{m} = \frac{2\pi r^2 \Sigma}{\dot{M}_E} \frac{\dot{r}}{r} = \frac{2\pi r^2 \Sigma(r)}{t_{\text{gw}}} \frac{1}{\dot{M}_E}. \quad (5)$$

Following Shakura & Sunyaev (1973), the standard disk structure has three distinct regions for a given accretion rate due to the source of opacity and pressure. In the inner region, the pressure and opacity of the disk are dominated by the radiation pressure and electron scattering, respectively. The pressure and opacity are dominated by the gas pressure and opacity of the electron scattering, respectively, in the middle region, whereas they are dominated by the gas pressure and opacity of the free-free absorption, respectively, in the outer region. At the present case, the outer region is neglected because the disk-outer edge is always less than the boundary between the middle region and the outer region. The surface density in the inner region and middle region is written by Kato et al. (2008) as

$$\Sigma(r) = \begin{cases} \Sigma_{\text{in}}(r/r_g)^{3/2} \dot{m}^{-1} & r \leq r_b \\ \Sigma_{\text{mid}}(r/r_g)^{-3/5} \dot{m}^{3/5} & r \geq r_b \end{cases}, \quad (6)$$

where  $\Sigma_{\text{in}} = 1.0 \times 10^3 \alpha_{0.1}^{-1} (1+q)^{3/2} f^{-1} [\text{g/cm}^2]$ ,  $\Sigma_{\text{mid}} = 4.3 \times 10^{31/5} \alpha_{0.1}^{-4/5} M_7^{1/5} (1+q)^{-4/5} f^{3/5} [\text{g/cm}^2]$  with  $f = 1 - \sqrt{3r_g/r}$ , and

$$\frac{r_b}{r_g} \approx 1.8 \times 10^{11/7} (\alpha_{0.1} M_7)^{2/21} \dot{m}^{16/21} (1+q)^{-23/21} \quad (7)$$

is the boundary between the inner region and the middle region.

A mass of accretion disk around the primary black hole at the decoupling is defined by  $M_{\text{ad}} = \int_{r_{\text{isco}}}^{r_{\text{o}}(\text{ad})} \Sigma(r) r dr$ , where  $r_{\text{isco}} = 3r_g/(1+q)$  shows the radius of innermost stable circular orbit around the Schwarzschild black hole. Since  $M_{\text{ad}}$  is an increasing function of black hole mass and  $M_{\text{ad}}/M_{\text{bh}} \lesssim 10^{-3}$  for  $M_{\text{bh}} = 10^8 M_\odot$  and  $q = 1$ ,  $M_{\text{ad}}$  is always less than  $M_{\text{sup}}$  over the whole mass range.

From equations (5) and (6), we finally obtain the normalized accretion rate as

$$\dot{m} = \begin{cases} \left[ (2\pi r_g^2 \Sigma_{\text{in}} / t_{\text{gw}}) \dot{M}_{\text{E}} \right]^{1/2} (r_{\text{o}}(a) / r_g)^{7/4} & r \leq r_{\text{b,o}} \\ \left[ (2\pi r_g^2 \Sigma_{\text{mid}} / t_{\text{gw}}) / \dot{M}_{\text{E}} \right]^{5/2} (r_{\text{o}}(a) / r_g)^{7/2} & r \geq r_{\text{b,o}} \end{cases}, \quad (8)$$

where  $r_{\text{b,o}}$  is a newly defined boundary between the inner region and middle region, which can be written as

$$\frac{r_{\text{b,o}}}{r_g} = \left[ \frac{16\pi}{5} \frac{q}{(1+q)^2} \frac{r_g c}{\dot{M}_{\text{E}}} \right]^{8/25} \frac{\Sigma_{\text{mid}}^{2/5}}{\Sigma_{\text{in}}^{2/25}}. \quad (9)$$

Note that the entire region of the disk is radiation-pressure dominated when  $r_{\text{o}}(a) \leq r_{\text{b,o}}$ .

The viscous timescale of the accretion disk around the primary black hole is written by  $t_{\text{vis}} \approx \sqrt{GM_{\text{bh}} r / (1+q)} / (\alpha_{\text{SS}} c_s^2)$ , where  $c_s$  is the sound velocity of the middle region of the disk. The ratio of  $t_{\text{vis}}$  to  $t_{\text{gw}}$  is then given by

$$\frac{t_{\text{vis}}}{t_{\text{gw}}} \sim (1+q) \left( \frac{r}{r_{\text{o}}(a)} \right)^{7/5}, \quad (10)$$

where equation (8) is substituted in the derivation process. Note that this ratio is independent of the viscosity parameter and black hole mass. The assumption that the disk is the steady state during the gravitational-wave driven evolution is thus justified in most of region of the disk because of  $t_{\text{vis}} \lesssim t_{\text{gw}}$ . From equation (10),  $t_{\text{vis}}$  is slightly longer than  $t_{\text{gw}}$  at the disk-outer edge. If the outer region of the disk is, however, hotter by the tidal dissipation,  $t_{\text{vis}}$  would become shorter than  $t_{\text{gw}}$ . In order to confirm whether this solution is realized, the time-dependent behavior including the effect of the tidal dissipation will be investigated in a subsequent paper.

Next, we consider that the disk becomes a bimodal system of standard disk-RIAF, where the standard disk in the cool outer region transits to the RIAF in the inner hot region. We employ a transition radius from the standard disk to the RIAF, which is defined by Homma (1996) as

$$\frac{r_{\text{t}}}{r_g} \approx 1.1 \times 10^{-2} \alpha_{0.1}^4 \epsilon_{0.1}^{-2} \dot{m}^{-2} (1+q)^{-1}. \quad (11)$$

The critical transition radius where the disk-outer edge corresponds to the transition radius is then written by using equation (2) and (8) as

$$\frac{r_{\text{t,c}}}{r_g} \sim 9.0 \times 10^{-1} \alpha_{0.1}^4 \epsilon_{0.1}^{-2} \frac{q}{(1+q)^{43/18}} \left( \frac{r_g c \Sigma_{\text{mid}}}{\dot{M}_{\text{E}}} \right)^{5/12}. \quad (12)$$



Note that the disk becomes the bimodal system when  $r_o(a) \leq r_{t,c}$ .

Fig. 1 shows the mass dependence of characteristic radii of the accretion disk in the binary with  $q = 0.1$ , and their evolution for  $M_{bh} = 10^7 M_\odot$ . All the radii are normalized by  $r_g$ . In panel (a), the solid line is the tidal radius when the binary is decoupled from the circumbinary disk. The dashed line and dotted line are  $r_{t,c}$  and  $r_{b,o}$ , respectively. Panel (a) shows  $r_{b,o} < r_{t,c} < r_o(a_d)$  in the range from  $10^5 M_\odot$  to  $10^8 M_\odot$ . In panel (b), the solid line, dashed line, and dotted line are  $r_o(a)$ ,  $r_t$ , and  $r_b$ , respectively. The intersection between the solid line and the dashed line represents  $r_{t,c}$ , whereas the one between the solid line and the dotted line shows  $r_{b,o}$ . It is noted from panel (b) that the disk becomes the RIAF before the disk is radiation-pressure dominated.

The luminosity of the RIAF normalized by the Eddington value can be written as(cf. Chap. 9 of Kato et al. 2008)  $L/L_E \approx \epsilon (\dot{m}/\dot{m}_c) \dot{m}$ , where  $\dot{m}_c \sim 1.0 \times 10^{-1} \epsilon_{0.1}^{-1} \alpha_{0.1}^2$  is the critical accretion rate normalized by  $\dot{M}_E$ . Note that there are no possible solutions of RIAFs for  $\dot{m} > \dot{m}_c$  (Narayan&Yi 1995). Fig. 2 shows the mass dependence of the normalized accretion rate and corresponding normalized luminosity in the binary with  $q = 0.1$ . The solid line and dashed line show the normalized accretion rate evaluated at the critical transition radius,  $\dot{m}_{RIAF}$ , and corresponding normalized luminosity,  $L_{RIAF}/L_E$ , respectively. The dotted line shows  $\dot{m}_c$ . It is clear from the figure that there is a possible solution for the RIAF because of  $\dot{m}_c > \dot{m}_{RIAF}$ . Both  $\dot{m}_{RIAF} \sim 2.0 - 3.0 \times 10^{-2}$  and  $L_{RIAF}/L_E \sim 5.0 - 9.0 \times 10^{-4}$  slightly decrease with the black hole mass in the range from  $10^5 M_\odot$  to  $10^8 M_\odot$ .

The virial temperature evaluated at the critical transition radius,  $T_{vir} \sim GM_{bh}m_p/r_{t,c}$ , is  $10^{10-11}$ K in the current-mass range. Such a high temperature disk can produce the X-ray emissions by the inverse Compton scattering and thermal bremsstrahlung, and radio emission by the synchrotron emission process. The luminosity of the synchrotron emission at the critical transition radius can be estimated by(Chap.6 of Rybicki&Lightman 1979)

$$\begin{aligned} \frac{L_{sync}}{L_E} &= \frac{2}{9} \frac{\sigma_T}{\dot{M}_E} \frac{\beta^2}{1 - \beta^2} n_e r_{t,c}^3 B^2 \\ &\sim 3.1 \times 10^{11/2} \eta_{0.1} \alpha_{0.1}^{-3/2} M_7^{-3/2} (1+q)^{1/4} \left( \frac{r_{t,c}}{r_g} \right)^{-17/4}, \end{aligned} \quad (13)$$

where  $\beta^2 = (r_{t,c}/r_g)^{-1}(1+q)^{-1}$ , the electron number density is evaluated by  $n_e \sim \Sigma(r_{t,c})/(m_p H)$ , where  $H$  is the disk-scale height, and magnetic field is evaluated by  $B \simeq 2.7 \times 10^5 \sqrt{\eta_{0.1}/M_7} (1+q)^{1/2} (r_{t,c}/r_g)^{-3}$ , based on an assumption of a dipole field with the strength of an equipartition value around a non-rotating black hole(Demer&Finke 2008). For the binary with  $10^7 M_\odot$  and  $q = 0.1$ ,  $L_{sync}/L_E \sim 5.0 \times 10^{-2}$ , which is significantly larger than that of other processes in the current case. This is a promising candidate as an electromagnetic counterpart of gravitational wave emitted at the black hole coalescence.

In an unequal mass-ratio binary, the critical transition radius of the disk around the primary black hole becomes larger than that of the secondary black hole. This difference causes step-like light variations in the radio emissions. Since the duration time approximately equals to the dynamical time evaluated at the critical transition radius, the difference of duration time can be written by  $\Delta t_{\text{duration}} = \sqrt{2}(r_g/c)(r_{\text{t,c}}/r_g)^{3/2}(1+q)^{1/2}(1-q^{5/6})$ . For the binary with  $M_{\text{bh}} = 10^7 M_\odot$  and  $q = 0.1$ , the difference of duration time becomes  $\Delta_{\text{duration}} \sim 2.0 \times 10^{-3}$  yr. On the other hand, the synchrotron-luminosity ratio of the secondary black hole to that of the primary black hole is  $L_{\text{sync,s}}/L_{\text{sync,p}} \simeq q^{-5/3}$ . For the binary with  $q = 0.1$ , the emission from the secondary black hole shows one-order of magnitude higher luminosity but shorter duration time than those of the primary black hole. The total light curve would thus exhibit step-like variations.

#### 4. Summary&Discussion

We study radiatively inefficient accretion flows onto each black hole during the gravitational-wave emission driven evolution of binary massive black holes in the framework of coevolution of massive black holes and their host galaxies.

The binary system initially consists of the accretion disk around each black hole and the massive circumbinary disk surrounding them. After the binary is decoupled from the circumbinary disk, the outer edge of each accretion disk shrinks with the orbital decay due to emission of gravitational wave. Assuming that the disk mass changed by the rapid orbital decay is all accreted, the accretion flow becomes radiatively inefficient when the disk-outer edge is less than the critical transition radius.

The bolometric luminosity corresponding to the accretion rate estimated at the critical radius is  $5.0 - 9.0 \times 10^{-4} L_E$  in the range from  $10^5 M_\odot$  to  $10^8 M_\odot$ . The RIAF produces X-ray emissions by the inverse Compton scattering and thermal bremsstrahlung, and radio emissions by the synchrotron process. Assuming that the magnetic field is a dipole field around a non-rotating black hole and its strength is the equipartition value, The radio emission by the synchrotron process is much more luminous than those of other processes and exhibits step-like variations by a sum of light curve from each component of the binary. Such a precursor implies that each accretion disk are drained because of the high energy radiation emitted by each disk prior to coalescence.

The peak frequency of the synchrotron emission is given by  $\nu_c = 3\gamma^2 eB \sin \alpha / (4\pi m_e c)$ , and  $\gamma$ ,  $m_e$ , and  $\alpha$  are the Lorentz factor, electron mass, and pitch angle between the magnetic field and the electron velocity, respectively. The peak-frequency ratio of the radiation emitted

by the disk around the secondary black hole to that of the primary black hole can then be estimated by  $\nu_{c,s}/\nu_{c,p} \simeq q^{-3/2}$  because the Lorenz factor and magnetic field strength depend on the mass ratio. The spectrum is therefore expected to have a double peak when one observe in a wide range of radio wavelengths.

A step-like nature of the light curve and double peak nature of the spectrum are unlikely to be seen in emissions from an accretion flow around a single massive black hole, and thus gives an unique photon diagnosis of binary black hole coalescences at large distances.

K.H. would like to thank anonymous referee for the useful comments and suggestions. K.H. is also grateful to Loeb Abraham, Shin Mineshige, and Takahiro Tanaka for helpful discussions. The calculations reported here were performed using the facility at the Centre for Astrophysics & Supercomputing at Swinburne University of Technology, Australia and at YITP in Kyoto University. This work has been supported by the Grants-in-Aid of the Ministry of Education, Science, Culture, and Sport and Technology (MEXT; 19740100, 18104003, 21540304, 22540243, 22340045).

## REFERENCES

- Abramowicz, M. A., Chen, X., Kato, S., Lasota, J.-P., & Regev, O. 1995, *ApJ*, 438, L37
- Armitage, P. J., & Natarajan, P. 2002, *ApJ*, 567, L9
- Begelman, M. C., Blandford, R. D., & Rees, M. J. 1980, *Nature*, 287, 307
- Berentzen, I., Preto, M., Berczik, P., Merritt, D., & Spurzem, R. 2009, *ApJ*, 695, 455
- Bode, T., Haas, R., Bogdanović, T., Laguna, P., & Shomarker, D. 2010, *ApJ*, 715, 1117
- Bogdanović, T., Smith, B. D., Sigurdsson, S., & Eracleous, M. 2008, *ApJ*, 174, 455
- Bogdanović, T., Eracleous, M., & Sigurdsson, S. 2009, *ApJ*, 697, 288
- Chang, P., Strubble, L.E., Menou, K., & Quataret E. 2009, arXiv0906.0825
- Cuadra, J., Armitage, P.J., Alexander, R.D., & Begelman, M.C. 2009, *MNRAS*, 393, 1423
- Corrales, L. R., Haiman, Z., & MacFadyen, A. 2010, *MNRAS*, 404, 947
- Dermer, C.D., & Finke, J.D. 2008, arXiv0810.1055
- Dotti, M., Colpi, M., Haardt, F., & Mayer, L. 2007, *MNRAS*, 379, 956

- Dotti, M., Montuori, C., Decarli, R., Volonteri, M., Colpi, M., & Haardt, F. 2009, MNRAS, 389, 73
- Escala, A., Larson, R.B., Coppi, P.S., & Mardones, D. 2005, ApJ, 630,152
- Ferrarese, L., & Merritt, D. 2000, ApJ, 539, L9
- Frank, J., King, A., & Raine, D. *Accretion Power in Astrophysics* 3rd ed., (Cambridge University Press 2002).
- Gould, A., & Rix, H. 2000, ApJ, 532, L29
- Gebhardt., K. et al. 2000, ApJ, 539, L13
- Haiman, Z., Kocsis, B., & Menou, K. 2009, ApJ, 700, 1952
- Hayasaki, K., Mineshige, S., & Ho, C.L. 2008, ApJ, 682, 1134
- Hayasaki, K., Mineshige, S., & Sudou, H. 2007, PASJ, 59, 427
- Hayasaki, K. 2009, PASJ, 61, 65
- Hayasaki, K., & Okazaki, A.T. 2009, ApJ, 691, L5
- Hayasaki, K., Ueda, Y., & Isobe, N. 2010, PASJ, 62, 1351
- Honma, F. 1996, PASJ, 48, 77
- Holz, E.D., & Hughes, A.S. 2005, ApJ, 629, 15
- Ichimaru, S. 1977, ApJ, 214, 840
- Ivanov, P. B., Papaloizou, J. C. B., & Polnarev, A. G. 1999, MNRAS, 307, 79
- Iwasawa, M., Funato, Y., & Makino, J. 2006, ApJ, 651, 1059
- Kato, S., Fukue, J., & Mineshige, S. *Black-Hole Accretion Disks*, (Kyoto Univ. Press. 2008).
- Kormendy, J., & Richstone, D. 1995, ARA&A, 33, 581
- Lodato, G., Nayakshin, S., King, A.R., & Pringle, J.E. 2009, 398, 1392
- Loeb, A. 2010, PhRvD, 81, 047503
- MacFadyen, I.A., & Milosavljević, M., 2008, ApJ, 672,83
- Magorrian, J., et al. 1998, AJ, 115, 2285

- Manmoto, T., Mineshige, S., & Kusunose, M. 1997, *ApJ*, 489, 791
- Matsui, M., & Habe, A. 2009, *PASJ*, 61, 421
- Mayer, L., Kazantzidis, S., Madau, P., Colpi, M., Quinn, T., & Wadsley, J. 2007, *Science*, 316, 1874
- Merritt, D., & Milosavljević, M. 2005, *Living Rev. Relativity*, 8, 8
- Milosavljević, M., & Phinney, E. S. 2005, *ApJ*, 622, L93
- Narayan, R., & Yi, I. 1994, *ApJ*, 428, L13
- Narayan, R., & Yi, I. 1995, *ApJ*, 452, 710
- Peters, P. C. 1964, *Physical Review*, 136, 1224
- Quinlan, G. D. 1996, *New Astron.* 1, 35
- Rybicki, G.B., & Lightman, A.P. 1979, *Radiation Process in Astrophysics* (NewYork: John Wiley & Sons, Inc)
- Rossi, E. M., Lodato, G., Armitage, P.J., Pringle, J.E., & King A. R. 2010, *MNRAS*, 401, 2021
- Shakura, N. I., & Sunyaev, R. A. 1973, *A&A*, 24, 337
- Schutz, B. F. 1986, *Nature*, 323, 310
- Stone, N., & Loeb, A. 2010, *arXiv:1004.4833*
- Tanaka, T., & Menou, K. 2010, *ApJ*, 714, 404